Insights into the high-sulphur aging of sintered silver nanoparticles
An experimental and ReaxFF study

Hu, Dong; Gu, Tijian ; Cui, Zhen; Vollebregt, Sten; Fan, Xuejun; Zhang, Guoqi ; Fan, Jiajie

DOI
10.1016/j.corsci.2021.109846

Publication date
2021

Document Version
Final published version

Published in
Corrosion Science

Citation (APA)
Hu, D., Gu, T., Cui, Z., Vollebregt, S., Fan, X., Zhang, G., & Fan, J. (2021). Insights into the high-sulphur aging of sintered silver nanoparticles: An experimental and ReaxFF study. *Corrosion Science*, *192*, 1-11. Article 109846. https://doi.org/10.1016/j.corsci.2021.109846

Corrosion Science 192 (2021) 109846

Contents lists available at ScienceDirect

Corrosion Science

journal homepage: www.elsevier.com/locate/corsci

Insights into the high-sulphur aging of sintered silver nanoparticles: An experimental and ReaxFF study

Dong Hu [b,1], Tijian Gu [c,1], Zhen Cui [b], Sten Vollebregt [b], Xuejun Fan [d], Guoqi Zhang [b], Jiajie Fan [a,b,*]

[a] Institute of Future Lighting, Academy for Engineering & Technology, Fudan University, Shanghai 200433, China
[b] Department of Microelectronics, Delft University of Technology, 2628 CD, Delft, The Netherlands
[c] College of Mechanical and Electrical Engineering, Hohai University, Changzhou 213022, China
[d] Department of Mechanical Engineering, Lamar University, Beaumont, TX 77710, USA

ARTICLE INFO

Keywords:
Silver
B. SEM
B. Modelling studies
C. Sulphidation
C. Oxidation
C. Interface

ABSTRACT

In high power electronics packaging, sintered silver nanoparticle joints suffer from thermal-humidity- electrical-chemical joint driven corrosion in extreme environments. In this paper, we conducted aging tests on sintered silver nanoparticles under high-temperature, high-humidity, and high-sulphur conditions. The results show that: (1) the sample under the dry high-sulphur conditions at a high temperature exhibited the highest degree of sulphidation; (2) Reactive force field (ReaxFF) molecular dynamics (MD) simulations of sintered silver nanoparticle sulphidation revealed the sulphidation layer was formed by silver atoms upward migration. This work paves the way for further investigation on sintered silver nanoparticles corrosion considering multi-physics coupling effects.

1. Introduction

More than Moore (MtM) refers to technology that is beyond the limitations of Moore's Law based upon or derived from silicon technologies [1]. As a key part of MtM, high power electronics technology is rapidly developing towards high power densities, more functionalization, and miniaturization. However, the harsh operating conditions create challenges for high electronics packaging [2,3]. Based on the restriction of hazardous substances (RoHS) directive, lead-free solders with great reliability at high temperatures are emerging [4,5]. Thus, an interconnection material with superior mechanical properties, electrical conductivity, and thermal dissipation ability is urgently required.

Recently, sintering nanomaterials, represented by silver nanomaterials, have received extensive attention [6]. Nano-silver materials have low sintering temperatures, and the sintered structures take advantage of the high melting point and excellent electrical and thermal conductivities. To date, extensive studies on nano-silver sintering have been carried out [7–10]. Joints sintered by silver nanoparticles (NPs) have been reported with excellent thermal and electrical properties compared to the commonly used Pb-free joints [11–13].

However, silver is prone to electrochemical migration behaviour [14] and suffers from tarnishing issues [15]. Corrosion failure thus becomes a severe issue for reliable performances [16]. Atmospheric corrosion of bulk silver has been widely studied [16,17]. Silver becomes tarnished at ambient pressure when exposed to atmospheric environments due to the presence of corrosive substances, such as SO_2, SO_3, O_2, and O_3 [18,19]. In addition, the influence factors, such as the relative humidity and concentrations of sulphur and ozone, have also been widely reported [20–22]. Furthermore, a considerate amount of literature has been published on silver tarnishing simulations. Despite the complex reactions, the adsorption site energetics for sulphur and oxygen on various silver surfaces have been calculated by density function theory [23]. Molecular dynamics (MD) simulations have high potential to handle large, complex simulation systems for silver tarnishing [24,25]. Reactive force field (ReaxFF) MD, as an empirical force field method to study chemical reactions, enriches the approximations with an adequate interatomic potential utilizing the reactive bond order [26]. Utilizing ReaxFF, Saleh et al. revealed the formation mechanism of silver oxide and silver sulphide and developed the related Ag/S and Ag/O force fields [27]. However, the corrosion in sintered silver nanoparticles

* Corresponding author at: Institute of Future Lighting, Academy for Engineering & Technology, Fudan University, Shanghai 200433, China,.
E-mail address: jiajie_fan@fudan.edu.cn (J. Fan).
[1] Dong Hu and Tijian Gu equally contribute to the present work.

https://doi.org/10.1016/j.corsci.2021.109846
Received 20 June 2021; Received in revised form 8 September 2021; Accepted 10 September 2021
Available online 16 September 2021

has barely been reported in experiments or simulations.

In this study, the pressure-assisted sintering of silver nanoparticles was performed, and the samples were divided into four groups to study the effects of high-temperature, high-humidity, and high-sulphur content on corrosion. The electrical conductivity and microstructural evolution were monitored to evaluate the corrosion degree. In addition, ReaxFF MD simulations were conducted to investigate the sulphidation behaviour in the sintered silver nanoparticles.

2. Experimental methodology

2.1. Sintering experiments

As shown in Fig. 1a, silver nanoparticles with an average particle size of 50 nm (Tide Powder) were used in this study. To obtain the sintered sample, a fixture and mould were self-designed, as shown in Fig. 1b. All the sintering experiments were then performed in a vacuum muffle furnace (SK3–5–12–10, Hangzhou Zhuochi Instrument Company) shown in Fig. 1c.(Fig. 2).

For each sample, 0.8 g of silver nanoparticles were weighed and then put into the designed mould. An auxiliary pressure of 30 MPa was applied by adjusting the fixture. After this, the packed mould was loaded into the furnace. The sintering profile adopted in this study is shown in Fig. 1d. The sample was heated at a rate of 6.25 °C/min to the maximum temperature of 275 °C. The dwell time was set to 50 min to promote sintering. After sintering, the sample was unmoulded and cooled at room temperature. The whole sintering process was performed in air.

2.2. High-sulphur aging experiments

To study the effects of high-sulphur and high-humidity environments on silver corrosion, four groups (A–D) were set up under different aging conditions, as presented in Table 1. To reduce the influence of random error, each group contained 30 samples, with sizes of 30 mm × 6 mm × 1 mm. All the groups were kept at 100 °C to accelerate the aging process. Furthermore, high-sulphur and high-humidity with 100% RH environments were used for groups B and C, respectively. In group D, both high-sulphur and high-humidity environments were introduced to investigate the coupled effect. Sulphur powder (Fig. 3a) was used as the pollutant for sulphidation corrosion.

In groups A and B, the samples were placed on glasses, which were loaded into the bottom of a stainless-steel reactor, as shown in Fig. 3b. For group B, there was an additional beaker containing sulphur powder in addition to the samples to create a high-sulphur environment. As for groups C and D, where high-humidity environment was considered, the aging reactions occurred in another type of reactor (Fig. 3c). The samples were placed in beakers and then put in a Teflon tank, which on bottom was filled with deionized water for group C and a mixture of deionized water and sulphur powder for group D. The packed Teflon tank was placed in the reactor. All the aging temperatures were controlled at 100 °C in the oven. The aging period was 168 h for each group.

2.3. Characterization methodology

To evaluate the corrosion degree, every 24 h, the electrical resistances of all the samples were measured, and two samples were removed for subsequent surface analysis. In terms of resistance

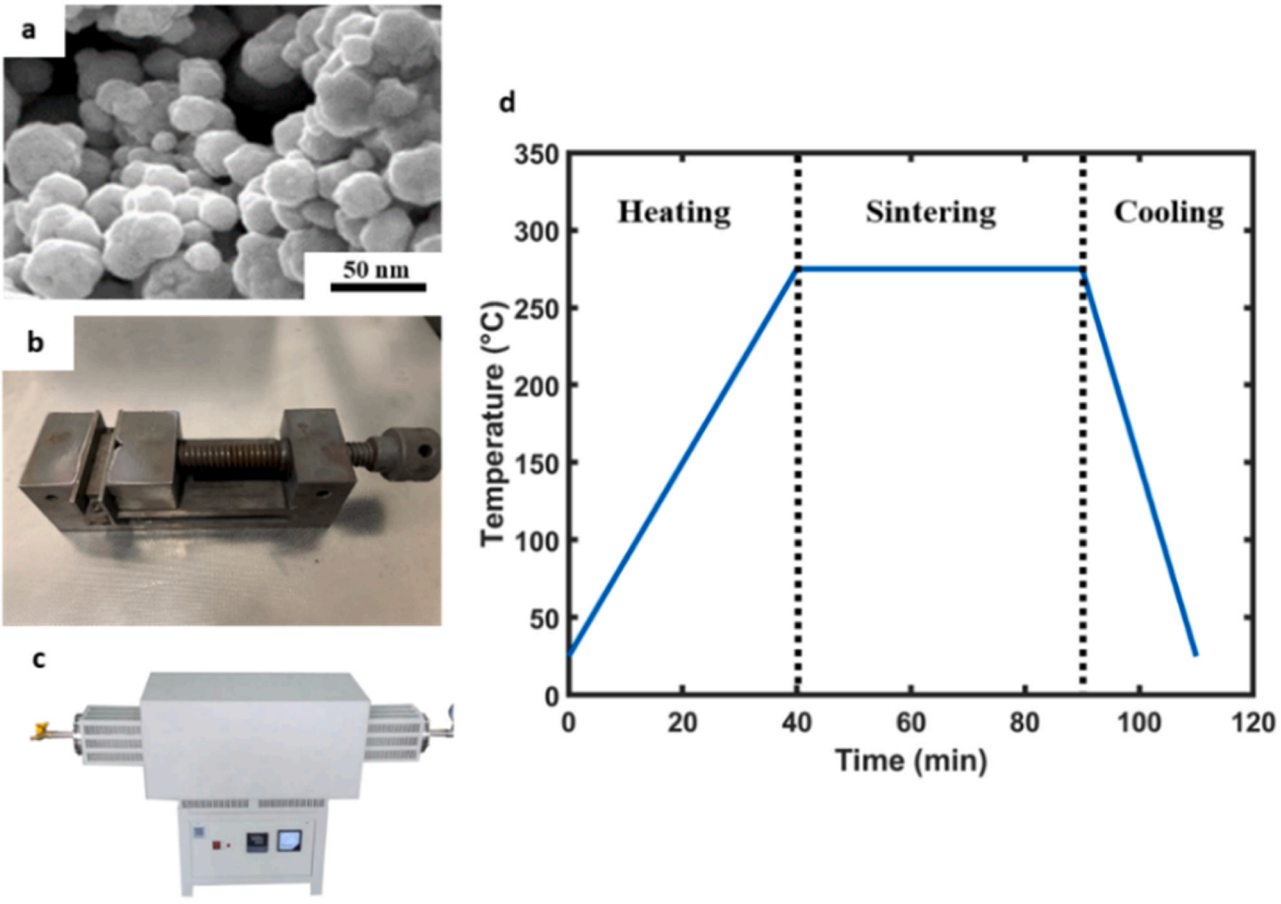

Fig. 1. (a) Purchased silver nanoparticles. (b) Self-designed fixture and mould. (c) Vacuum muffle furnace. (d) Temperature profile of low-temperature sintering.

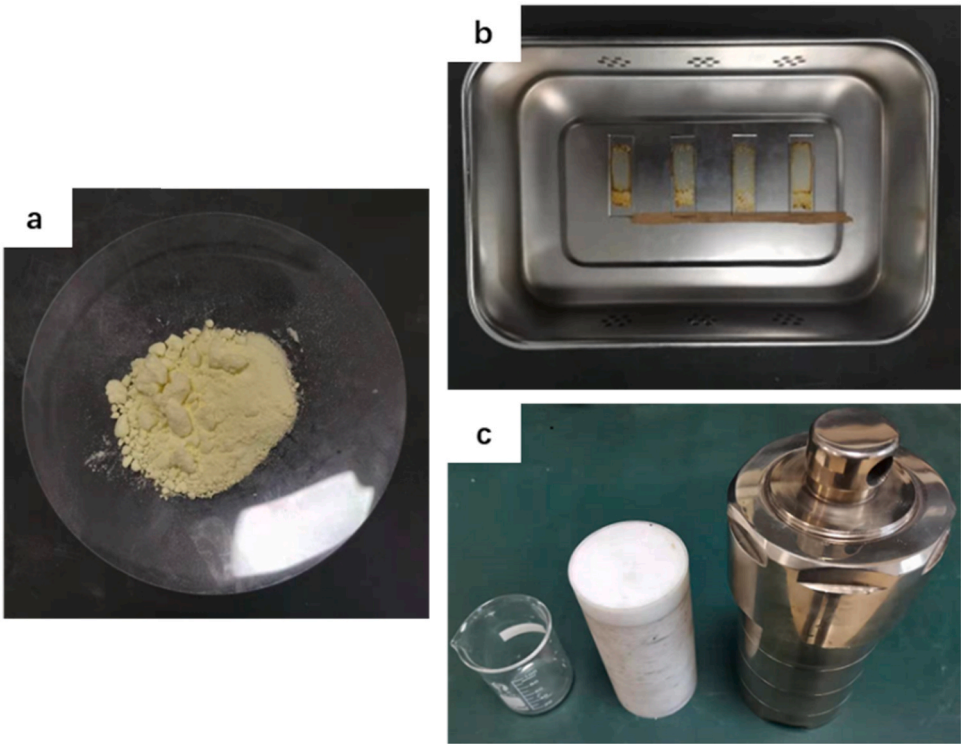

Fig. 2. (a) S_8 powder, (b) non-high-humidity environment reactor, and (c) high-humidity environment reactor.

Table 1
Overview of the aging conditions used in this study.

Group No.	High Temperature (100 °C)	High sulphur	High humidity (100% RH)
A	√	–	–
B	√	√	–
C	√	–	√
D	√	√	√

measurements, a power supply (Keithley 2200) was employed to generate a 1-A direct current for larger voltage signal due to the excellent electrical conductivity of silver. Meanwhile, the instantaneous resistance was measured by a multimeter (Keysight 34411 A). The surfaces and cross sections were observed by scanning electron microscopy (SEM, JSM-6360). Energy-dispersive X-ray spectroscopy (EDX, Qualtec) was performed to determine the composition in the target area.

3. Computational methods

3.1. MD methodology

In this study, MD simulations of the pressure-assisted sintering of silver nanoparticles and further sulphidation were conducted. The Large-scale Atomic/Molecular Massively Parallel Simulator (LAMMPs) was employed to conduct all the simulations [28]. The configurations were visualized using three-dimensional visualization software, the Open Visualization Tool (OVITO) [29].

To simulate the pressure-assisted sintering, the classical embedded atom method (EAM) potential developed by Foiles et al. [30] was applied to describe the interactions between Ag atoms. This EAM potential has been proven to be able to calculate properties, such as the cohesive energy, phase diagram, lattice constant, and elastic constant of silver atoms, accurately. The total energy E_{tot} can be expressed as follows [31]:

$$E_{tot} = \sum_i F_i(\rho_{h,i}) + \frac{1}{2}\sum_i \sum_{j(\neq i)} \varnothing_{ij}(R_{ij}), \quad (1)$$

where $\rho_{h,i}$ is the host electron density of atom i, $F_i(\rho)$ is the energy to embed atom i into the background electron density ρ, and $\varnothing_{ij}(R_{ij})$ is the core–core pair repulsion between atoms i and j with a distance of R_{ij}.

However, the EAM is not capable of describing reactive chemistry, such as bond formation and breaking of bonds. The ReaxFF with the Ag/S parameters developed by Saleh et al. [27] was adopted in this study. This force field has been confirmed to describe the sulphurisation behaviour on an Ag slab surface correctly. The total energy term in the ReaxFF force field can be expressed as follows [32]:

$$E_{system} = E_{bond} + E_{over} + E_{under} + E_{H-bond} + E_{lp} + E_{val} + E_{tors} + E_{vdWaals} + E_{Coulomb}. \quad (2)$$

The total energy of the system consisted of bond-order-dependent or covalent interactions and non-bonded interactions. Bond-order-dependent terms include the bond energy (E_{bond}), over coordination (E_{over}), undercoordination (E_{under}), and hydrogen bond interactions (E_{H-bond}). Energy penalty terms include the torsion angle energy (E_{tors}), valence angle energy (E_{val}), and lone pair energy (E_{lp}), whereas the non-bonded terms are the van der Waals energy ($E_{vdWaals}$) and Coulomb energy ($E_{Coulomb}$).

3.2. Simulation details

All the systems simulated in this study adopted periodic boundaries, and the conjugate gradient algorithm was used for energy minimization. To simulate the pressure-assisted sintering, a symmetric multi-Ag nanoparticle system was established, containing 15,688 atoms in total. The diameter of each Ag nanoparticle was 3.6 nm, and the atomic spacing was set at 3.5 Å. The dimensions of the simulation cell were 80 Å × 80 Å × 80 Å. The system was relaxed using the NVE (microcanonical) ensemble at 300 K for 100 ps. The system was then heated from 300 to 575 K within 500 ps using the NPT (isothermal–isobaric)

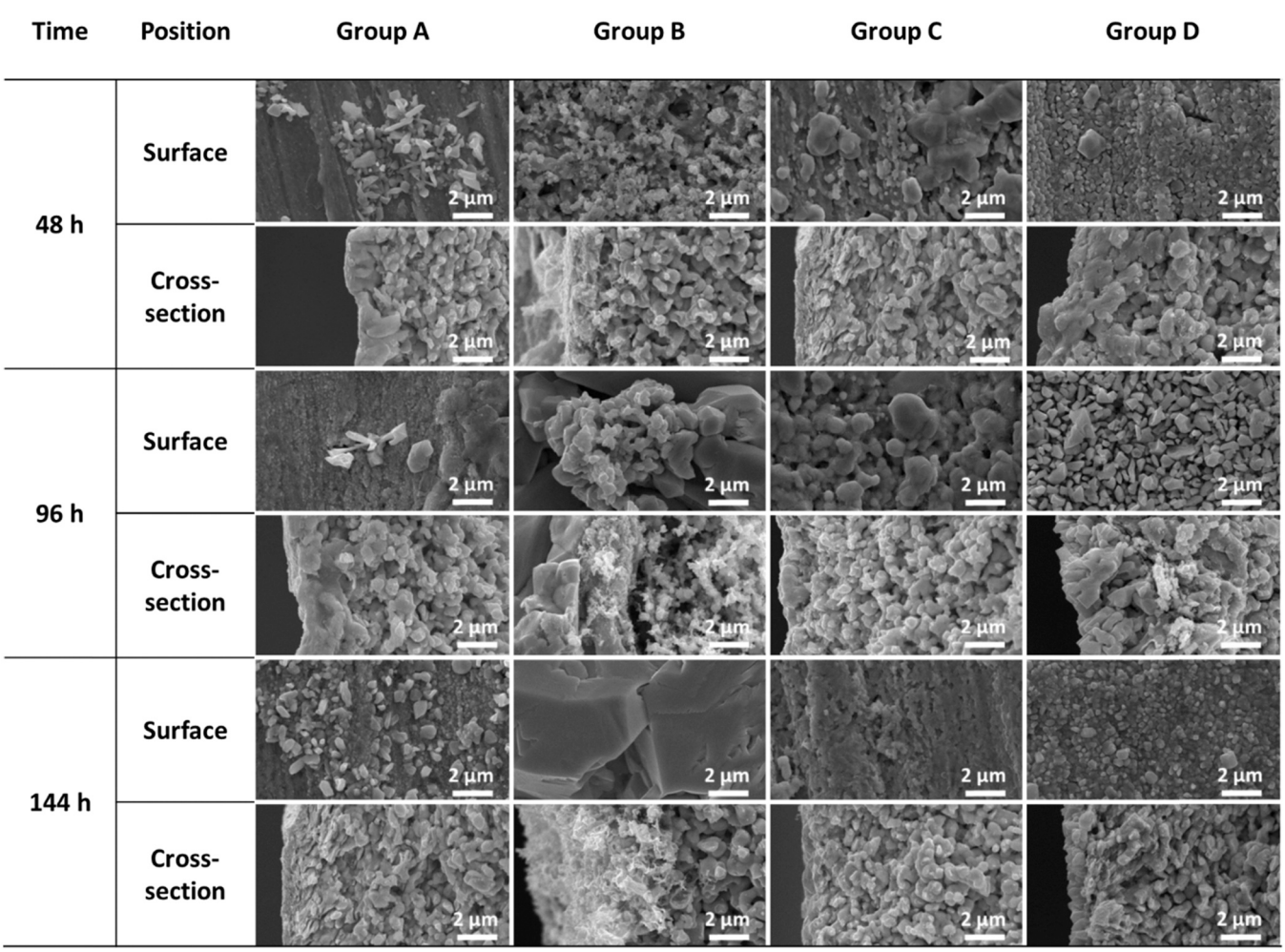

Fig. 3. Surface and cross-sectional SEM images of the sintered Ag samples exposed to different aging conditions for 48, 96, and 144 h.

ensemble by controlling the pressure on the simulation box to 30 MPa. To promote the sintering, an extra 1.5-ns dwell period was included, which also used the NPT ensemble at a constant 30 MPa. Eventually, the sintered structure cooled to room temperature (300 K) in another 500 ps. Meanwhile, the pressure on the box was released to atmospheric pressure.

The NVT ensemble was employed to simulate sulphurisation. Temperatures were controlled through the Nose–Hoover thermostat. The time step was chosen as 0.5 fs, and the damping constant was selected as 100 fs. Two temperatures, 373 and 750 K, were selected to investigate the effect of temperature. At first, atoms were assigned random velocities at the target temperature, with a Gaussian distribution. The system was then kept at the target temperature for 500 ps for further reaction and sulphur diffusion. Trajectories were analysed by the mean-square displacement (MSD), defined as follows:

$$\mathrm{MSD} = \frac{1}{N}\sum_{i=1}^{N}\left|r^i(t) - r^i(0)\right|^2, \tag{3}$$

where N is the number of particles, t is the time, and $r^i(t) - r^i(0)$ is the vector distance travelled by atom i.

4. Results and discussion

4.1. Morphological characterization

The morphological evolutions of the different group samples exposed for 48, 96, and 148 h were inspected by SEM, and the results are shown in Fig. 3. The samples of groups A and C showed similar results. From the surface morphology, several dendritic corrosion products were evident, but they did not cover the whole surface. Furthermore, the sizes and number of the corrosion products did not extensively change during longer exposure. However, in the sample from group B, a large number of agglomerated amorphous features appeared. When the exposure increased to 96 h, a large amount of sulphide product appeared around the agglomeration regions of the sintered Ag. Upon further sulphidation, at an exposure time of 144 h, a large sulphide crystal was observed, indicating a high degree of sulphidation on the outer surface. In contrast, in the sample from group D, small crystals were found at the exposure time of 96 h. However, the sulphidation products did not further grow into large crystals, but a uniform corrosion layer was formed.

The results for the cross section were consistent with the surface morphology changes. In groups A and C, a thin corrosion layer was observed, and its thickness did not increase with longer exposure. However, in the samples exposed to a high-sulphur environment, a thick corrosion layer was observed. Group B experienced the highest degree of corrosion at 48 h, and an interface was formed between the corrosion products and the sintered Ag. At 96 h, corrosion product rupture at the

interface was evident, as well as the appearance of a large sulphide crystal. The cross section at 144 h exhibited a delaminated surface on which the sintered Ag was covered by a uniform layer of amorphous features. In addition, in group D, no delamination was observed because large corrosion product crystals had not formed. Consequently, at 144 h, a solid and uniform corrosion layer formed with a thickness of ~1 μm.

Furthermore, EDX was performed on the cross section at 48 and 144 h to detect the presence of the corrosion products shown in Fig. 4. On each cross section, two areas were selected, one in the body of the sintered Ag and the other at the surface. The results were consistent with the morphological results. In the areas in the body of the sintered Ag, no evident corrosion products were detected. Furthermore, in the groups under the aging conditions without sulphur, the corrosion product contents were negligible on the surface at both 48 and 144 h. In contrast, in group B, at 48 h, no sulphur was detected on the surface, but 9.16 at% sulphur was detected in the sample at 144 h. In group D, at 48 h, sulphidation products were present on the surface with 4.29 at% sulphur. However, this content of sulphur did not increase, and as a result, at 144 h, the surface corrosion products contained 4.87 at% sulphur.

The results presented above suggested that the aging condition without sulphur resulted in limited corrosion products. Furthermore, the presence of high humidity was likely to slow down the formation of large sulphide crystals.

4.2. Resistivity analysis

Fig. 5 shows the resistivity evolution throughout the tests, where the error bars represent standard deviations. As a reference, the average resistivity of the sample at 0 h was 1.64×10^{-4} Ω•cm. As shown in Fig. 5a, the resistivities of the samples in group B significantly increased due to the presence of sulphur vapour. The vapour pressure is estimated by the Antoine equation as 13.8 Pa at 100 °C [33]. The evolution of the sample resistivity can be divided into three stages. In the first stage before 48 h, the resistivity grew steadily to 4.57×10^{-4} Ω•cm. Then, a sudden increase to 6.79×10^{-3} Ω•cm was recorded from 48 to 144 h, indicating a faster corrosion rate. Consequently, the increase in the resistivity slowed and reached 7.17×10^{-3} Ω•cm at 168 h, which was 43 times higher than that of the uncorroded sample. In group A, the curve was almost flat, and the resistivity slightly increased to 2.31×10^{-4} Ω•cm after 168 h of corrosion at a high temperature. Thus, the presence of sulphur vapour in a dry environment enabled a significant increase in the resistivity, indicating a high corrosion rate.

To investigate the influence of sulphur vapour with the presence of moisture-saturated air, the resistivity changes were plotted, as shown in Fig. 5b. A large gap between the two groups was also observed. In group D, the development of the resistivity also underwent three stages. First, it followed a growing trend, gradually increasing to 6.4×10^{-4} Ω•cm at 48 h. A plateau appeared after 48 h, where the resistivity was almost unchanged. After 96 h, the resistivity began to rapidly increase and consequently reached 2.44×10^{-3} Ω•cm at 168 h, nearly 14 times the initial value. However, in group C, with the high humidity, the resistivity changed gradually during the whole test process until 120 h. After this, it experienced a slight increase to 2.11×10^{-4} Ω•cm at 168 h. Therefore, under high-humidity aging conditions, the presence of sulphur vapour also enabled severe corrosion.

Thus, in the groups containing sulphur vapour, the conductivity degradation was significant. There is a huge difference between the resistivities of silver oxide (~50 Ω•cm) and silver sulphide (~1 MΩ•cm) [34,35]. In addition, under an O_2 exposure environment, the molecular or atomic oxygen is only chemisorbed on the surface instead of being quickly incorporated into the silver [36], whereas the chemisorption of molecular or atomic sulphur on the silver surface is stronger

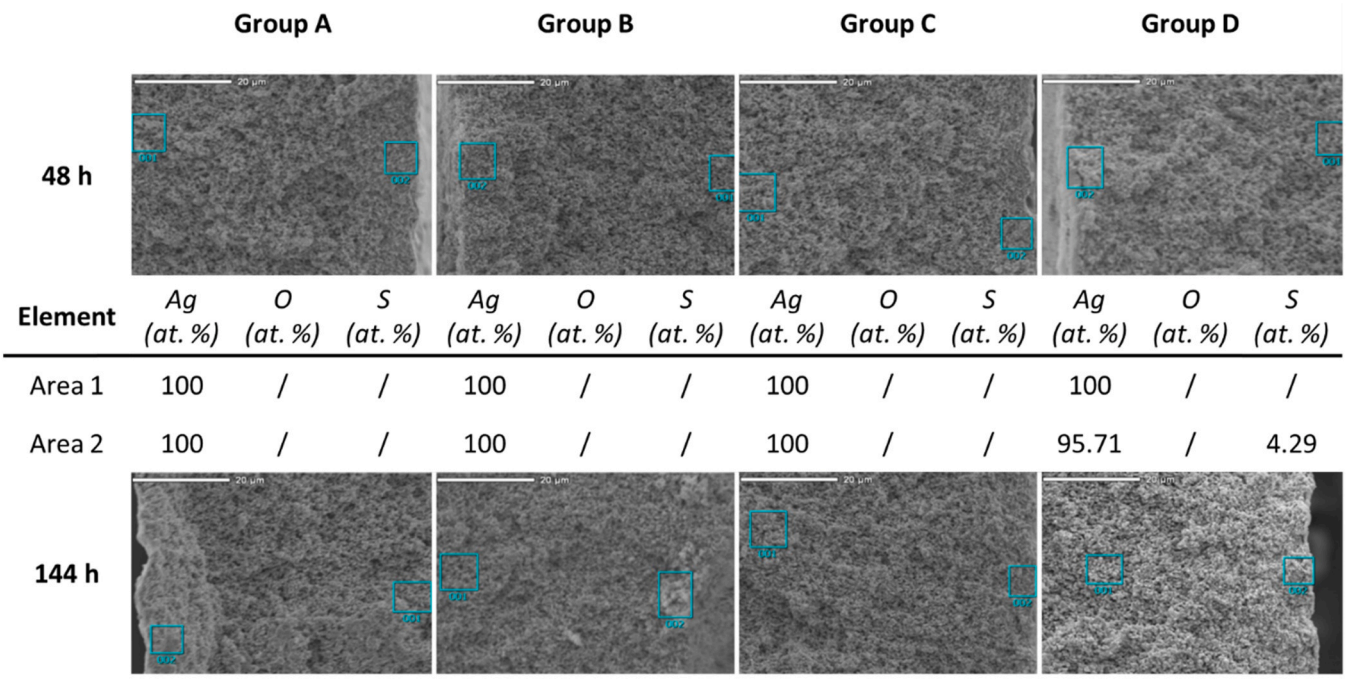

Fig. 4. Energy-dispersive X-ray spectroscopy (EDX) results of material compositions for samples under different aging conditions at 48 and 144 h.

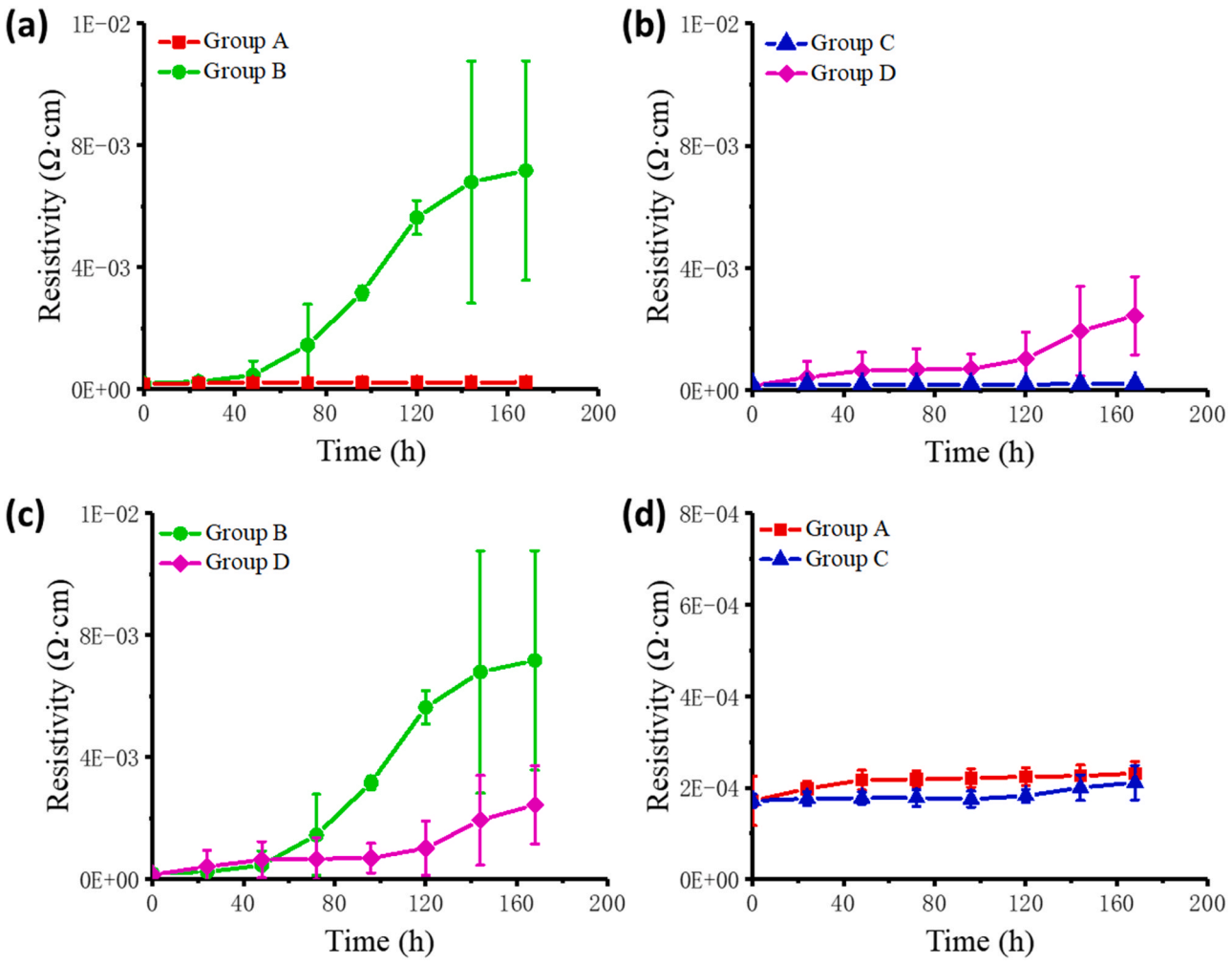

Fig. 5. Evolution of resistivity under different aging conditions: (a) effect of sulphur vapour in a dry environment, (b) effect of sulphur vapour in a wet environment, (c) effect of humidity on sulphur vapour, and (d) effect of humidity without sulphur vapour.

than that on oxygen [37].

In Fig. 5c, by comparing the resistivity evolution in groups B and D, the effect of high humidity on the sulphidation was studied. Before 48 h, the resistivity of the two groups showed few deviations. However, from 48 to 120 h, the conductivity of group B showed significant degradation, while there was a plateau in group D. Consequently, at 168 h, the resistivity of group D was one-third of the resistivity of group B, indicating that less corrosion occurred. This result was consistent with the morphological characterization results mentioned before, where less sulphur was detected on the sample surface. Thus, moisture slowed the sulphidation corrosion in the sintered Ag nanoparticles. This may have been because, in the case of S_8 as a pollutant, high humidity inhibited the diffusion of oxygen and sulphur near the outer surface [38].

Finally, under the aging condition without sulphur, the resistivity experienced 40.9% and 28.7% increases in groups A and C, respectively, as shown in Fig. 5d. These results were in agreement with the morphological characterization results for these groups described above, which showed limited corrosion degrees and slight differences between the surface and cross-sectional images.

The abovementioned results suggest that under atmospheric aging conditions at 100 °C, sintered Ag is not significantly oxidized by O_2. Furthermore, the humidity plays an insignificant role in the corrosion of sintered Ag at 100 °C, both for oxidation or sulphidation corrosion.

4.3. Molecular dynamics simulations

4.3.1. Atomic model construction

As the 30-MPa pressure-assisted sintering process occurred, atoms travelled to the necking area between the nanoparticles, and a dense structure was obtained. The initial configuration and the configuration of the sintered system are shown in Fig. 6a. The sintering degree was characterized by the evolution of the MSD, as shown in Fig. 6b. When pressure was applied, the NPs quickly sintered at 300 K. The MSD then increased as the temperature increased. Consequently, the MSD became stable during the 300-K relaxation process, indicating that a stable sintered microstructure was formed. The density of the sintered microstructure was 5.95 g/cm^3, which was 56.7% of the value of bulk Ag.

In the sulphurisation simulations, to reduce the computational cost, one-fourth of the sintered structure was extracted for further simulation. Meanwhile, a single crystal of Ag with the same dimensions was created. An 80-Å vacuum layer was added on the top and bottom sides, where 150 S_8 molecules were randomly placed. The S_8 molecule was selected here because, according to the experiments, most sulphur vapour molecules were in the form of S_8, and it was previously reported that the aging condition with sulphur vapour is more severe than that with hydrogen sulphide gas [39]. The S_8 molecule was pre-relaxed at 750 K for 50 ps. Every added S_8 molecule maintained a distance of not less than 3 Å with any existing atom. The assembled system shown in Fig. 6c had a size of 38.7 Å × 38.7 Å × 237.7 Å, containing 4529 and 7189 atoms, respectively, for the model with the sintered Ag and the bulk Ag.

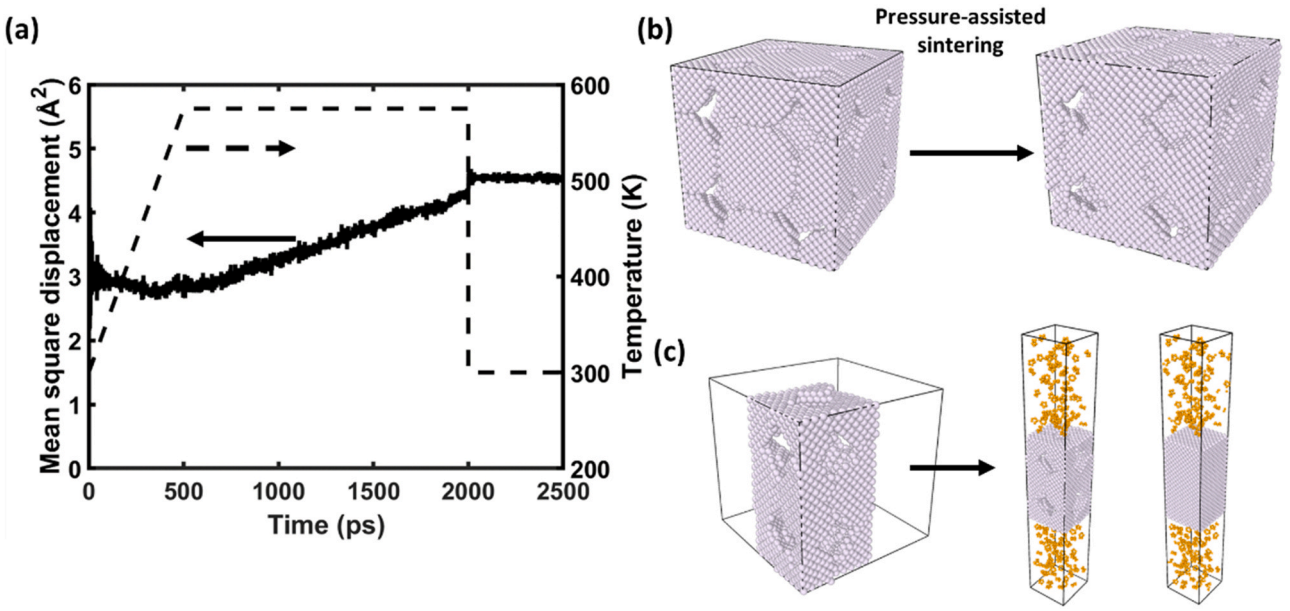

Fig. 6. Pressure-assisted sintering: (a) mean-square displacement (MSD) and temperature evolution, (b) atomic configuration evolution, and (c) atomic configuration for sulphidation simulation.

Silver and sulphur atoms are coloured silver and orange, respectively.

4.3.2. Sulphurisation simulations

The reaction mechanism of sulphide was revealed to be the following. First, sulphur molecules physisorbed on the surface of the silver, where significant charge exchange did not occur. Next, S_8 dissociation occurred on the surface and resulted in chemisorbed S atoms by reaction with Ag. Then, the thickening of the sulphide layer was not only contributed to by the S atoms diffusing into the Ag layer but surface Ag atoms were also dragged out of their original positions and continuously migrated upwards. As shown in Fig. 7, a selected Ag atom was lifted by one atomic layer in a short period. The reaction was confirmed by the change in the atomic charge. The atomic charge rapidly increased from 0.158*e* to 0.263*e* in 2.5 ps and then remained stable, indicating an equilibrium state. The resulting vacancy was then filled with S atoms. This result is consistent with previous reports [40, 41]. The formation of surface sulphides was the main reason for the electrical resistance degradation.

4.3.2.1. Porous structure effect. To investigate the influence of porous structures on sulphur corrosion, models with different microstructures were simulated at 750 K for 500 ps. Silver sulphidation occurred at the surface, and the sulphide layer was formed by the diffusion as well as the upward migration of silver atoms. Eventually, a thicker sulphide layer was found in the model with sintered Ag after 500 ps. The thickness of the sulphide layer was defined as the distance between the lowest and topmost silver atoms along the z-axis. The atomistic configuration after sulphurisation, as well as the evolution of the sulphide layer thickness, is shown in Fig. 8a.

At the end of the simulation, the thicknesses of the sulphide layer in the model with sintered Ag and the model with single-crystal Ag were 25.3 and 11.2 Å, respectively, as shown in Fig. 8b. The steady increase rate had a minor difference between the two models. This was because the diffusivity of sulphur in silver was based on the intrinsic properties of the material, which was independent of the porous structure.

The greater sulphidation corrosion in the sintered Ag was attributed to two factors. When the simulation began, a non-uniform sulphide layer abruptly formed. This was confirmed by the cross section snapshots shown in Fig. 9. A sulphur molecule (coloured red) quickly diffused into the pore within 3 ps. It then climbed around on the inner surface for a short time and then adsorbed on the surface. Meanwhile, the sulphidation on the surface was ongoing. Consequently, it reacted with the Ag atoms in the pore, as dissociation of the S_8 molecule was observed.

In addition, in the model with sintered Ag, sulphurisation lasted longer, while in the model with single-crystal Ag, the thickness of the sulphide layer became stable after 370 ps. This was because the porous structure had more reaction sites than the defect-free structure. The sulphidation corrosion was an electrochemical reaction with electron exchange between silver and sulphur atoms. Thus, the degree of sulphidation could be described by the evolution of the total charge of the sulphur atoms, as shown in Fig. 10a. According to the slope of the charge evolution, the model with sintered Ag exhibited more electrochemical activity. As a result, after the 500 ps simulation, the model with single-crystal Ag lost 135.1 *e* worth of charge, while this number was more than

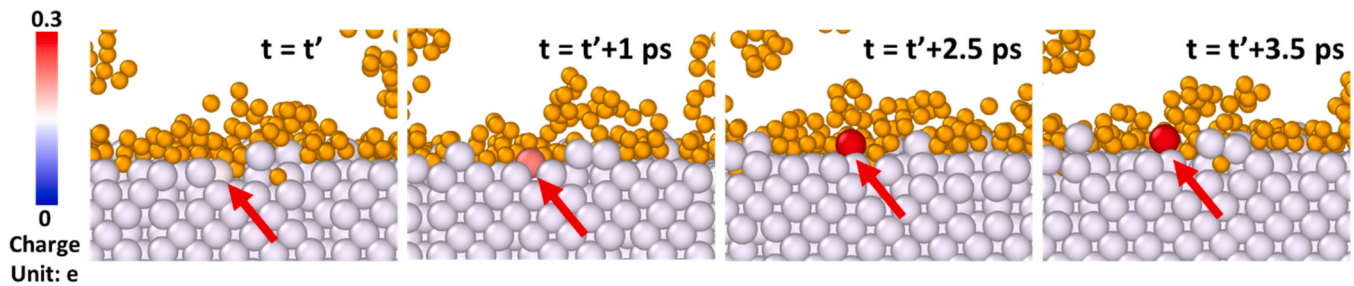

Fig. 7. Ag sulphidation mechanism for surface Ag atoms. Only a selected Ag atom is coloured based on its atomic charge.

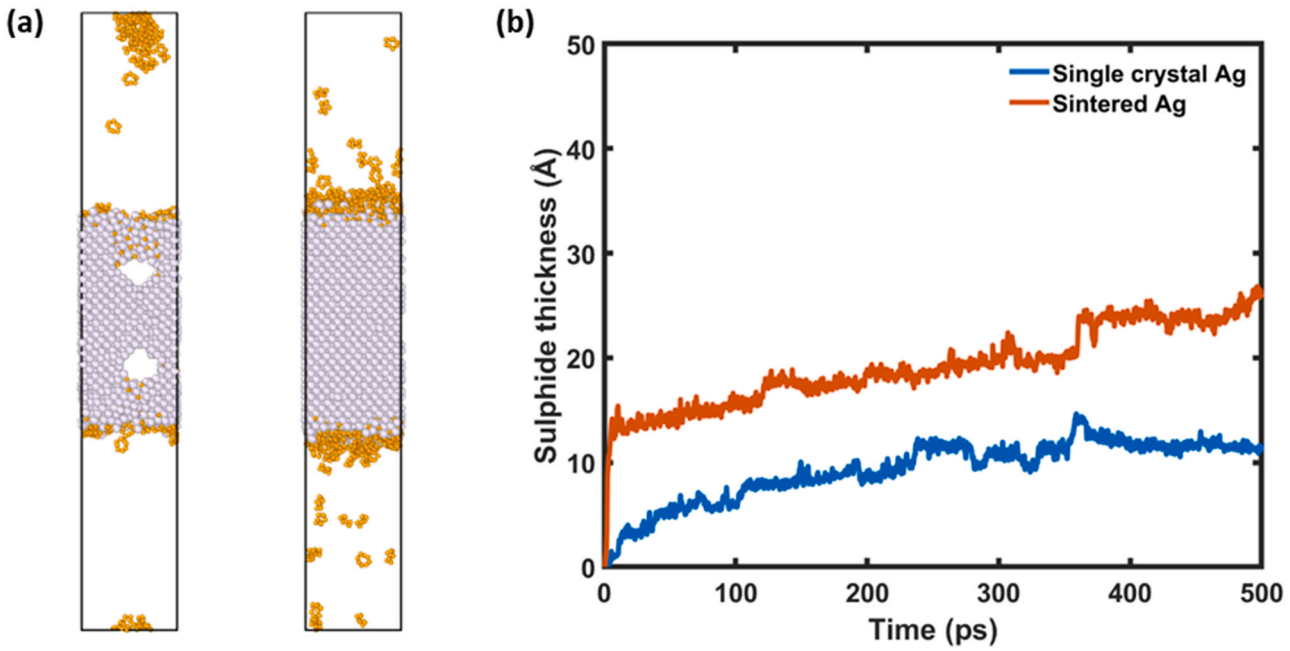

Fig. 8. Formation of silver sulphide layer: (a) atomistic configuration after 500 ps and (b) evolution of sulphide layer thickness.

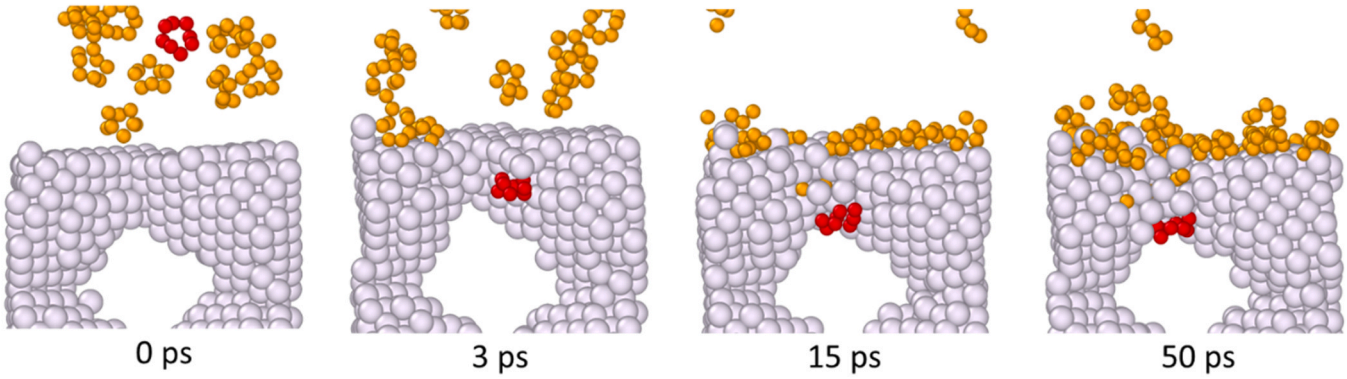

Fig. 9. Snapshots for the fast formation of sulphide layer at the beginning of the simulation (cross section).

double in the model with sintered Ag (295.6 *e*). This result was consistent with the abovementioned difference in thickness. Furthermore, the distribution of silver and sulphur atoms along the x-axis after the simulation is shown in Fig. 10b. In the model with single-crystal Ag, the distribution of sulphur and silver atoms shared the same trend. The area with fewer atoms was contributed to by the sulphidation process, wherein the silver continuously diffused into the sulphide layer [40]. However, in the model with sintered Ag, due to the existence of pores, fewer Ag atoms were present in the middle area. In contrast, S atoms were better distributed in this area, indicating the accumulation of S atoms in the pores. Thus, the sintered Ag showed more significant sulphidation corrosion due to the greater number of reaction sites created by the pores.

4.3.2.2. Temperature effect. Furthermore, the effect of temperature on the sulphidation was also investigated. For the model with sintered Ag, another sulphidation simulation at 373 K (100 °C) was conducted. The post-sulphidation atomistic configuration and the evolution of the sulphide layer thickness are shown in Fig. 11a.(Fig. 12).

A large number of S_8 molecules accumulated on the outer surface of the sintered silver awaiting further reaction. As a result, the final sulphide layer thickness at 373 K was 14.2 Å, while this number was 25.3 Å at 750 K. In Fig. 9b, a rapid increase at the beginning of the simulation was found at both temperatures. However, the sulphidation rate at 373 K was slower than that at 750 K. In the case of 373 K, the growth of sulphide layer formed several plateaus during the sulphidation. This explains the non-uniformity of the sulphide layer. The evolution of the charge difference showed that the total charge transfer at 373 K was 12.99 *e*, which was 1/22 the value at 750 K. This indicated that less sulphidation occurred at 373 K, and the reaction rate was much slower. To directly view the distribution of S atoms, the atomic coordinates along the Z-axis are shown in Fig. 11b. In the histogram of the Ag atoms, the lower bars indicate the positions of the pores. At 373 K, the overlapping region between the S and Ag atoms mainly existed at the edge. Thus, it was confirmed that the S_8 molecule that diffused into the pore did not diffuse further, and at this moment, most of the sulphide formed at the outer surface. In contrast, at 750 K, there were more overlapping bars, which meant that more sulphide formed as well as diffused S atoms in Ag body. Therefore, it was concluded that higher temperature could extensively accelerate the growth of the sulphide layer, resulting in greater sulphidation corrosion.

In summary, the sulphidation corrosion on silver depended on the microstructure as well as the sulphidation temperature. The sintered Ag was prone to sulphidation corrosion due to its porous structure. Sulphur

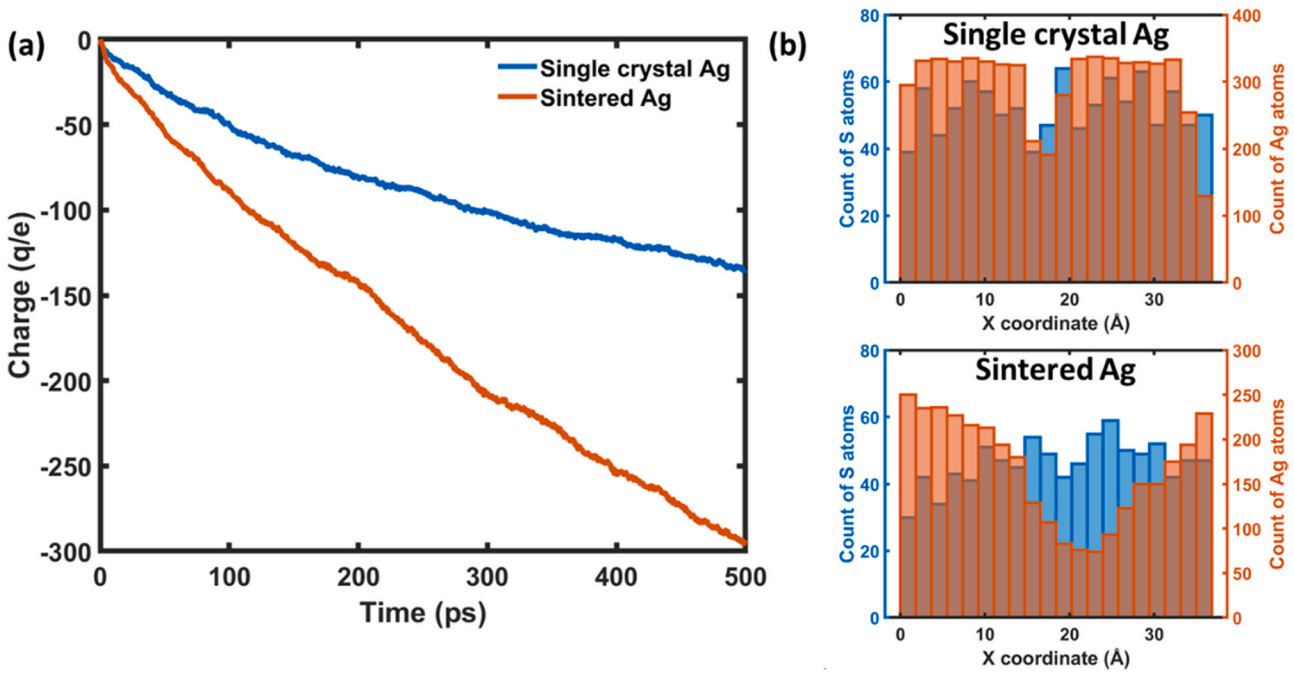

Fig. 10. Sulphidation process: (a) evolution of total charge of Ag atoms and (b) atom position along the X-axis.

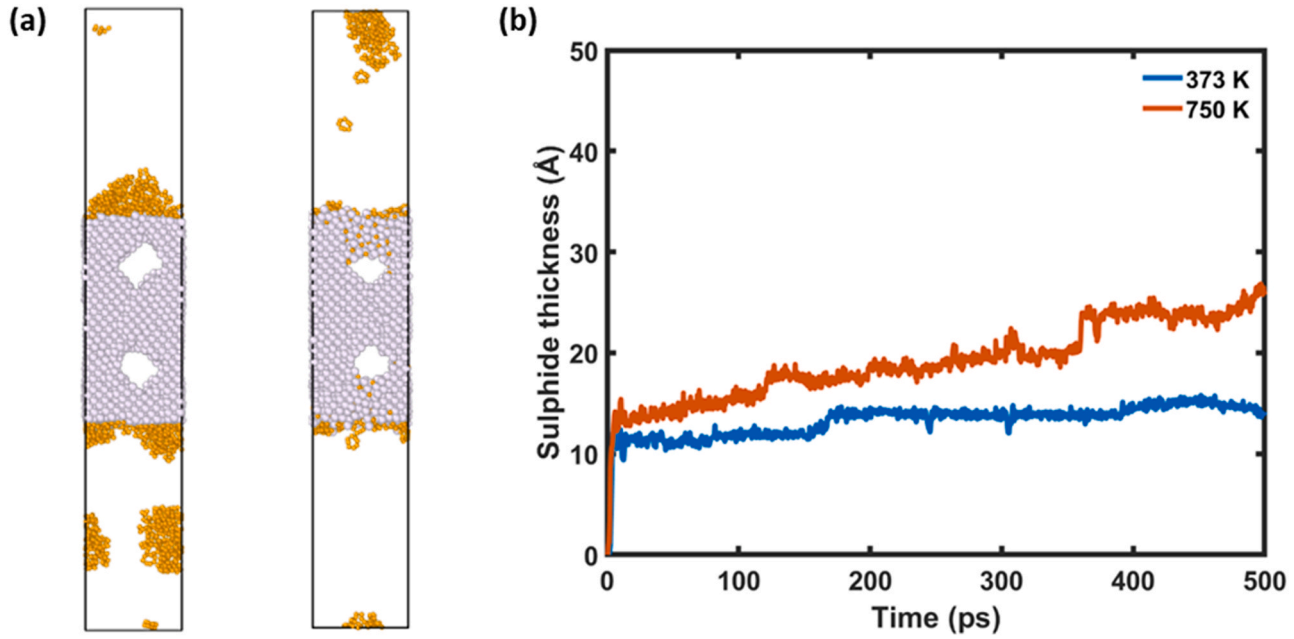

Fig. 11. Formation of silver sulphide layer: (a) atomistic configuration after 500 ps and (b) evolution of sulphide layer thickness.

molecules can transport into the sintered Ag body through pores and react on the inner surface. Besides, high sulphidation temperature extensively promotes the sulphidation rate. The practical applications of power electronics packaging, such as in electrical vehicles and the power grid, are usually at high operating temperatures. Thus, sulphidation corrosion is an important factor that should be considered during package design.

5. Conclusion

In this paper, the aging of sintered silver nanoparticles under high-temperature (100 °C), high-sulphur (13.8 Pa), and high-humidity (100% RH) aging conditions was conducted. The degradation was evaluated by monitoring the electrical resistivity and microstructural evolution. The results can be concluded as: Firstly, the sintered samples were highly corroded in the high-sulphur environment at high temperature with the presence of a layer of crystalline sulphide. Furthermore, the samples in the high-humidity environment exhibited less corrosion compared to the samples in the dry environment. Moreover, ReaxFF MD simulations were performed to examine the sulphidation on the sintered silver nanoparticles. The sulphidation mechanism was revealed to be the upward migration of surface silver atoms to the sulphur-rich layer as well as sulphur atom diffusion into the silver body. In addition, the porous structure suffered more severe sulphidation due to large inner surface area. The pore was found to have slight effect on the sulphidation rate, whereas the aging temperature was a dominant factor.

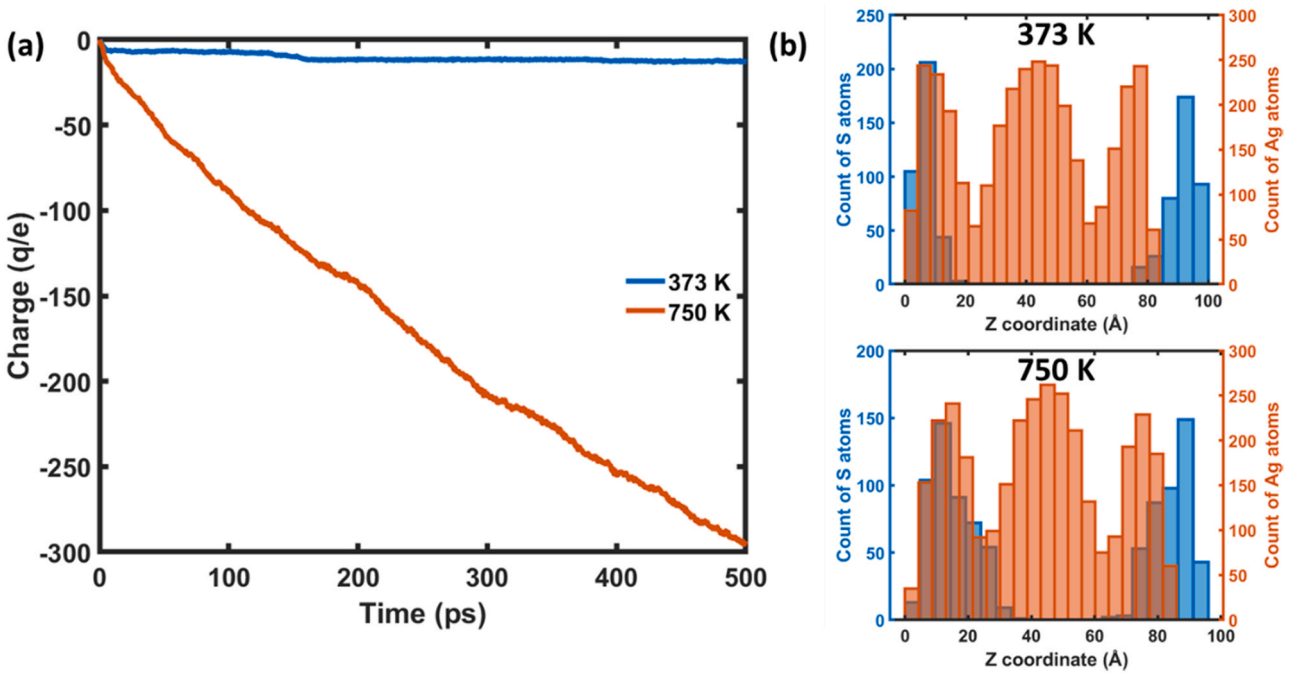

Fig. 12. Sulphidation process: (a) evolution of total charge of Ag atoms and (b) atom position along Z-axis.

CRediT authorship contribution statement

Dong Hu: Simulation and analysis; Writing – original draft. **Tijian Gu**: Experiments, Data collection and analysis. **Zhen Cui**: Technical supports on simulation, **Sten Vollebregt**: Supervision. **Xuejun Fan**: Supervision. **Guoqi Zhang**: Supervision. **Jiajie Fan**: Conceptualization, Methodology, Writing – review & editing, Project administration, Funding acquisition, Supervision.

Declaration of Competing Interest

The authors declare that they have no known competing financial interests or personal relationships that could have appeared to influence the work reported in this paper.

Acknowledgements

This work was supported by National Natural Science Foundation of China, China (51805147) and the Six Talent Peaks Project in Jiangsu Province, China (GDZB-017).

References

[1] G.Q. Zhang, M. Graef, F. Van Roosmalen, The rationale and paradigm of "More than Moore", Proc. - Electron. Compon. Technol. Conf. 2006 (2006) 151–157, https://doi.org/10.1109/ECTC.2006.1645639.
[2] A. Abuelnaga, M. Narimani, A.S. Bahman, A review on IGBT module failure modes and lifetime testing, IEEE Access 9 (2021) 9643–9663, https://doi.org/10.1109/ACCESS.2021.3049738.
[3] H. Wang, F. Blaabjerg, K. Ma, Publish and prosper reader response to "White Hot" column in March 2016 issue of the magazine, IEEE Power Electron. Mag. 3 (2016) 13.
[4] A. Kar, M. Ghosh, R.N. Ghosh, B.S. Majumdar, A.K. Ray, Evolution of mechanical and electrical properties of tin-lead and lead free solder to copper joint interface, Mater. Lett. 62 (2008) 151–154, https://doi.org/10.1016/j.matlet.2007.04.116.
[5] H. Wang, H. Zhao, D.P. Sekulic, Y. Qian, A comparative study of reactive wetting of lead and lead-free solders on cu and (Cu 6Sn 5/Cu 3Sn)/Cu substrates, J. Electron. Mater. 37 (2008) 1640–1647, https://doi.org/10.1007/s11664-008-0502-8.
[6] S.A. Paknejad, S.H. Mannan, Review of silver nanoparticle based die attach materials for high power/temperature applications, Microelectron. Reliab. 70 (2017) 1–11, https://doi.org/10.1016/j.microrel.2017.01.010.
[7] G. Zou, J. Yan, F. Mu, A. Wu, J. Ren, A. Hu, Y.N. Zhou, Low temperature bonding of Cu metal through sintering of Ag nanoparticles for high temperature electronic application low temperature bonding of Cu metal through sintering of Ag nanoparticles for high temperature electronic application, Open Surf. J. 3 (2011) 70–75, https://doi.org/10.2174/1876531901103010070.
[8] H. Zhang, G. Zou, L. Liu, A. Wu, Y.N. Zhou, Low temperature sintering of silver nanoparticle paste for electronic packaging, in: 2016 Int. Conf. Electron. Packag., The Japan Institute of Electronics Packaging, 2016: pp. 314–317. https://doi.org/10.1109/ICEP.2016.7486837.
[9] H. Yu, L. Li, Y. Zhang, Silver nanoparticle-based thermal interface materials with ultra-low thermal resistance for power electronics applications, Scr. Mater. 66 (2012) 931–934, https://doi.org/10.1016/j.scriptamat.2012.02.037.
[10] T. Wang, X. Chen, G.Q. Lu, G.Y. Lei, Low-temperature sintering with nano-silver paste in die-attached interconnection, J. Electron. Mater. 36 (2007) 1333–1340, https://doi.org/10.1007/s11664-007-0230-5.
[11] Z.Z. Zhang, G.Q. Lu, Pressure-assisted low-temperature sintering of silver paste as an alternative die-attach solution to solder reflow, IEEE Trans. Electron. Packag. Manuf. 25 (2002) 279–283, https://doi.org/10.1109/TEPM.2002.807719.
[12] B.H. Lee, M.Z. Ng, A.A. Zinn, C.L. Gan, Application of Copper Nanoparticles as Die Attachment for High Power LED, in: 2015 IEEE 17th Electron. Packag. Technol. Conf., 2015: pp. 1–5.
[13] T. Fujimoto, T. Ogura, T. Sano, M. Takahashi, A. Hirose, Joining of pure copper using Cu nanoparticles derived from CuO paste, Mater. Trans. 56 (2015) 992–996.
[14] B. Medgyes, B. Illés, G. Harsányi, Electrochemical migration behaviour of Cu, Sn, Ag and Sn63/Pb37, J. Mater. Sci. Mater. Electron. 23 (2012) 551–556, https://doi.org/10.1007/s10854-011-0435-5.
[15] J. Ortíz-Corona, J.L. Ruvalcaba-Sil, E. Casanova-González, F.J. Rodríguez-Gómez, Surface analysis of the tarnishing layer in silver alloys, MRS Adv. 357 (2017) 1–8, https://doi.org/10.1557/adv.201.
[16] H. Han, X. Dong, H. Lai, H. Yan, K. Zhang, J. Liu, P.J. Verlinden, Z. Liang, H. Shen, Analysis of the degradation of monocrystalline silicon photovoltaic modules after long-term exposure for 18 years in a hot-humid climate in China, IEEE J. Photovolt. 8 (2018) 806–812, https://doi.org/10.1109/JPHOTOV.2018.2819803.
[17] T.E. Graedel, Corrosion mechanisms for silver exposed to the atmosphere, J. Electrochem. Soc. 139 (1992) 1963–1970, https://doi.org/10.1149/1.2221162.
[18] C.J. Yang, C.H. Liang, X. Liu, Tarnishing of silver in environments with sulphur contamination, Anti-Corros. Methods Mater. 54 (2007) 21–26, https://doi.org/10.1108/00035590710717357.
[19] A. García-Segura, A. Fernández-García, M.J. Ariza, F. Sutter, P. Watermeyer, M. Schmücker, L. Valenzuela, Corrosion on silvered-glass solar reflectors exposed to accelerated aging tests with polluting gases: A microscopic study, Corros. Sci. 176 (2020), 108928, https://doi.org/10.1016/j.corsci.2020.108928.
[20] Y. Salem, The influence of gaseous pollutants on silver artifacts tarnishing, Open J. Air Pollut. 06 (2017) 135–148, https://doi.org/10.4236/ojap.2017.64011.
[21] R. Wiesinger, I. Martina, C. Kleber, M. Schreiner, Influence of relative humidity and ozone on atmospheric silver corrosion, Corros. Sci. 77 (2013) 69–76, https://doi.org/10.1016/j.corsci.2013.07.028.
[22] I. Martina, R. Wiesinger, M. Schreiner, Micro-Raman investigations of early stage silver corrosion products occurring in sulfur containing atmospheres, J. Raman Spectrosc. 44 (2013) 770–775, https://doi.org/10.1002/jrs.4276.

[23] D.J. Liu, P.A. Thiel, Oxygen and sulfur adsorption on vicinal surfaces of copper and silver: preferred adsorption sites, J. Chem. Phys. 148 (2018), 124706, https://doi.org/10.1063/1.5021091.
[24] M. He, X. Liu, X. Lu, C. Zhang, R. Wang, Structures and acidity constants of silver-sulfide complexes in hydrothermal fluids: a first-principles molecular dynamics study, J. Phys. Chem. A. 120 (2016) 8435–8443, https://doi.org/10.1021/acs.jpca.6b08403.
[25] S.I. Sadovnikov, I.A. Balyakin, Molecular dynamics simulations of zinc sulfide deposition on silver sulfide from aqueous solution, Comput. Mater. Sci. 184 (2020), 109821, https://doi.org/10.1016/j.commatsci.2020.109821.
[26] T.P. Senftle, S. Hong, M.M. Islam, S.B. Kylasa, Y. Zheng, Y.K. Shin, C. Junkermeier, R. Engel-Herbert, M.J. Janik, H.M. Aktulga, T. Verstraelen, A. Grama, A.C.T. Van Duin, The ReaxFF reactive force-field: Development, applications and future directions, Npj Comput. Mater. 2 (2016) 15011, https://doi.org/10.1038/npjcompumats.2015.11.
[27] G. Saleh, C. Xu, S. Sanvito, Silver tarnishing mechanism revealed by molecular dynamics simulations, Angew. Chem. - Int. Ed. 58 (2019) 6017–6021, https://doi.org/10.1002/anie.201901630.
[28] S. Plimpton, Fast parallel algorithms for short-range molecular dynamics, J. Comput. Phys. 117 (1995) 1–19, https://doi.org/10.1006/jcph.1995.1039.
[29] A. Stukowski, Visualization and analysis of atomistic simulation data with OVITO – the Open Visualization Tool, Model. Simul. Mater. Sci. Eng. 18 (2010), 015012, https://doi.org/10.1088/0965-0393/18/1/015012.
[30] S.M. Foiles, M.I. Baskes, M.S. Daw, Embedded-atom-method functions for the fcc metals Cu, Ag, Au, Ni, Pd, Pt, and their alloys, Phys. Rev. B. 33 (1986) 7983–7991, https://doi.org/10.1103/PhysRevB.33.7983.
[31] M.S. Daw, S.M. Foiles, M.I. Baskes, The embedded-atom method: a review of theory and applications, Mater. Sci. Rep. 9 (1993) 251–310, https://doi.org/10.1016/0920-2307(93)90001-U.
[32] A.C.T. Van Duin, S. Dasgupta, F. Lorant, W.A. Goddard, ReaxFF: a reactive force field for hydrocarbons, J. Phys. Chem. A. 105 (2001) 9396–9409, https://doi.org/10.1021/jp004368u.
[33] J.A. Dean. Lange's Handbook of Chemistry, 15th ed., McGraw-Hill, New York, USA, 1999.
[34] A. Tvarusko, The electric resistivity of AgO, J. Electrochem. Soc. 115 (1968) 1105, https://doi.org/10.1149/1.2410919.
[35] S. Banerjee, S. Bhattacharya, D. Chakravorty, Resistivity hysteresis of AgS nanocomposites resistivity hysteresis of Ag2S nanocomposites, J. Phys. Chem. 111 (2007) 13410–13413.
[36] G.I.N. Waterhouse, G.A. Bowmaker, J.B. Metson, Oxidation of a polycrystalline silver foil by reaction with ozone, Appl. Surf. Sci. 183 (2001) 191–204, https://doi.org/10.1016/S0169-4332(01)00561-X.
[37] N. Islam, D.C. Ghosh, The electronegativity and the global hardness are periodic properties of atoms, J. Quantum Inf. Sci. 01 (2011) 135–141, https://doi.org/10.4236/jqis.2011.13019.
[38] B.T. Reagor, J.D. Sinclair, Tarnishing of silver by sulfur vapor: film characteristics and humidity effects, J. Electrochem. Soc. 128 (1981) 701–705, https://doi.org/10.1149/1.2127485.
[39] Y. Huo, S.W. Fu, Y.L. Chen, C.C. Lee, A reaction study of sulfur vapor with silver and silver–indium solid solution as a tarnishing test method, J. Mater. Sci. Mater. Electron. 27 (2016) 10382–10392, https://doi.org/10.1007/s10854-016-5124-y.
[40] I. Bartkowicz, S. owec, Ionic conductance of silver sulphide and diffusion mechanism of silver ions in α-Ag2S, Phys. Status Solidi 49 (1972) 101–105, https://doi.org/10.1002/pssb.2220490108.
[41] J.F. Fan, G.C. Yang, Y.H. Zhou, Y.H. Wei, B.S. Xu, Selective oxidation and the third-element effect on the oxidation of Mg-Y alloys at high temperatures, Metall. Mater. Trans. A Phys. Metall. Mater. Sci. 40 (2009) 2184–2189, https://doi.org/10.1007/s11661-009-9874-5.